Supplementary Information for

Synergistic dual-defect band engineering for highly-efficient photocatalytic degradation of microplastics via Nb-induced oxygen vacancies in SnO_2 quantum dots

Jianqiao Liu[1,4], Dan Zhao[2], Xian Wu[1], Di Wu[1], Ningning Su[1], Yang Wang[1], Fang Chen[3], Ce Fu[1,*], Junsheng Wang[1,*], Qianru Zhang[4,*]

1. College of Information Science and Technology, Dalian Maritime University, Dalian 116026, Liaoning, China P.R.

2. School of Transportation, Department of Roadway Engineering, Southeast University, Nanjing, 211189, Jiangsu, China P.R.

3. Center of Advanced Optoelectronic Materials, College of Materials and Environmental Engineering, Hangzhou Dianzi University, Hangzhou, 310018, China

4. Institute of Agriculture Resources and Regional Planning, Chinese Academy of Agricultural Sciences, Beijing 100081, China P.R.

***Corresponding author:** Ce Fu, Junsheng Wang and Qianru Zhang

Email: fuce_dlmu@sina.com (C. Fu), wangjsh@dlmu.edu.cn (J. Wang) and zhangqianru@caas.cn (Q. Zhang)

Tel: +86 411 84729934 **Fax:** +86 411 84729934

Address: College of Information Science and Technology, Dalian Maritime University, Linghai Road 1, Ganjingzi District, Dalian 116026, Liaoning, China P.R.

Supplementary Text

Characterizations of photocatalysts

The undoped and Nb-doped SnO_2 QDs were characterized in terms of their microstructure, elemental composition, and morphology. The crystal structures were determined by using X-ray diffraction (XRD, Empyrean, Malvern Panalytical, Netherlands) with Cu Kα radiation. The elemental bondings and valence states were evaluated by X-ray photoelectron spectroscopy (XPS, ESCALAB 250XI, ThermoFisher Scientific, US). All peaks are calibrated using the C 1s peak at 284.8 eV. The microstructure and morphology were observed by high-resolution transmission electron microscopy (HRTEM, JEM-2100F, JEOL, Japan). The spatial distribution of each element was collected by high-angle annular dark-field scanning transmission electron microscopy (HAADF-STEM, FEI-Talos F200s, ThermoFisher Scientific, US). The ultraviolet-visible (UV-Vis) absorption was examined by a UV7600 spectrophotometer (Lengguang Technology, Shanghai, China). The photoluminescence properties were evaluated using a fluorescence spectrophotometer (F96Pro, Lengguang Technology, Shanghai, China) with excitation wavelength of 280 nm. Time-resolved photoluminescence (TRPL) spectra were collected by the transient fluorescence spectrometer (FLS 980, Edinburgh Instruments, UK) to evaluate the fluorescence lifetime of carriers. The inductively coupled plasma optical emission spectrometer (ICP-OES, Optima 8300, PerkinElmer, USA) was used to determine the actual Nb doping amount in SnO_2 matrix. The Electron Spin Resonance (ESR) spectra were recorded using a JES-FA300 spectrometer (JEOL, Tokyo, Japan) functioned at an X-band frequency, utilizing a 100 kHz modulation frequency and a 9.86 GHz microwave frequency.

Evaluation of photocatalytic properties

The photocatalytic properties of undoped and Nb-doped SnO_2 QDs were evaluated by the visible-light driven degradation of methyl orange (MO) dye at room temperature. 1 mL of SnO_2 QD solution containing 0.2 mol/L Sn

atoms and 40 mL MO solution at a concentration of 30 mg/L were mixed into a quartz vessel. The mixture was stirred in the dark for 30 minutes to establish adsorption-desorption equilibrium between the photocatalysts and MO dye. A white LED array of 8 W, emitting light in the range of 400-800 nm, was used as the light source for irradiation. During the photocatalytic process, aliquots of the target solution were centrifuged, and the supernatant was analyzed by UV-Vis absorption. The concentration of MO was determined based on the intensity of the absorption peak using the Lambert-Beer law. The degradation efficiency and rate constant were calculated using Eqs. (S1) and (S2), respectively.

$$\text{MO Efficiency}(\%) = \frac{C_0 - C}{C_0} \times 100\% \tag{S1}$$

$$\ln(\frac{C}{C_0}) = -kt \tag{S2}$$

Here, C_0 was the initial concentration of MO and C was the MO concentration at a certain time during photocatalytic process. k and t were rate constant and time, respectively. The bandgap (E_g) of Nb-doped SnO_2 QDs was determined by evaluating the Tauc plot relation based on the UV-Vis absorbance. The position of valence band edge (E_V) was determined by the XPS valence spectrum. The position of conduction band edge (E_C) was calculated by E_C=E_V-E_g.

Optimization of photocatalytic properties

Fig. S10(a) illustrates the degradation process of MO dye during photocatalytic activities, and the corresponding degradation efficiency is calculated and presented in Fig. S10(b). The photocatalysts, incorporating Nb at levels of 3% to 9%, demonstrate highly efficient degradation abilities, achieving a degradation efficiency of over 97% within 25 minutes at room temperature. Among these catalysts, 6%Nb-SnO_2 exhibits the best performance, as it had the lowest likelihood of electron-hole recombination. The rate constants of photocatalysis are calculated and listed in Table S5. The relationship between the rate constants and Nb incorporation is depicted in Fig. S10(b). The

degradation of MO dye occurs in two steps with different rate constants, denoted as k_1 and k_2, as shown in Fig. S10(b). According to the pathway of MO degradation, the rate constant k_1 represents the initial degradation process from MO (m/z=304) to the intermediate product P9 (m/z=308). The degradation activity is accelerated by the double routes from P9 to the final products, as indicated by the rate constant k_2. Compared to the undoped SnO_2 QDs, the 6%Nb-SnO_2 photocatalyst enhances k_1 by 6.25 times and k_2 by 56.08 times, respectively.

Fig. S11(a) shows the Zeta potentials of samples, which falls between -41 mV and -37 mV. These values guarantee excellent stability of QD photocatalysts in aqueous solution. Fig. S11(b) exhibits the long-term performances of Zeta potentials and degradation ability of 6%Nb-SnO_2 QDs. In a period of 90 days, both of Zeta potential and degradation efficiency of MO show decreases by approximate 16.3% and 6.2%, respectively, indicating good long-term stability of 6%Nb-SnO_2 QDs in aqueous environment.

Determination of primary active radicals

To identify the primary active radicals in the photocatalytic degradation process led by 6%Nb-doped SnO_2 QDs, the radical scavengers of IPA, $KBrO_3$, $(NH_4)_2C_2O_4$ and BQ are employed to capture the respective active radicals of $^{\bullet}OH$, e^-, h^+ and $O_2^{\bullet-}$ during photocatalytic activities. The trapping experiments, as shown in Fig. S17, indicate the presence of all four active radicals in the photocatalytic activities. It is also found that $^{\bullet}OH$ is the primary active radical driving the photocatalytic process facilitated by Nb-doped SnO_2 QDs. The generation of $^{\bullet}OH$ radicals is attributed to the oxidation of water, resulting from the combination of photo-generated holes and OH^- anions. The band structures of Nb-doped SnO_2 QDs, shown in Fig. 2(c), demonstrate that the E_V position over 3 eV ensures a strong oxidizing ability of the photo-generated holes. Thus, it can be concluded that$^{\bullet}OH$ radicals play a crucial role in the photocatalytic activities of Nb-doped SnO_2 QDs.

Supplementary Figures

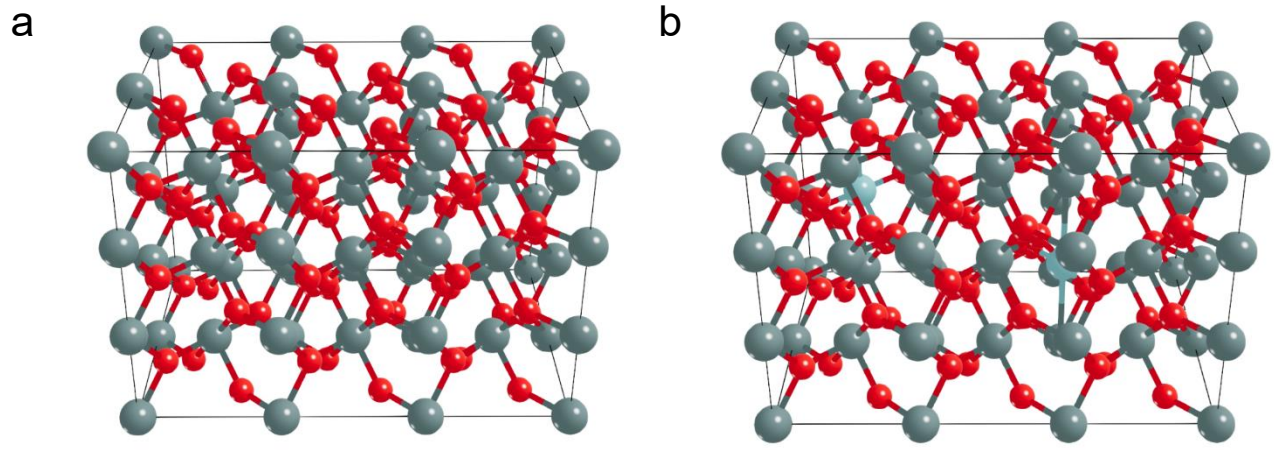

Fig. S1 Schematic illustration of (a) the undoped SnO_2 super cell with 7 oxygen vacancies and (b) the Nb-doped SnO_2 super cell with 12 oxygen vacancies and 2 Sn atoms substituted by Nb. Grey for Sn, red for O and light green for Nb atoms.

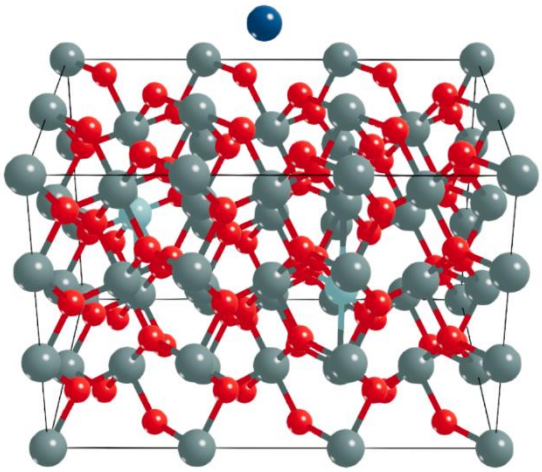

Fig. S2 Schematic illustration of absorption of metal cations (Na^+, K^+, Ca^{2+}, Mg^{2+}, Zn^{2+}, Cu^{2+}, Fe^{3+} and Al^{3+}) on the Nb-doped oxygen-deficient SnO_2 super cell. Grey for Sn, red for O, light green for Nb and dark blue for metal atoms.

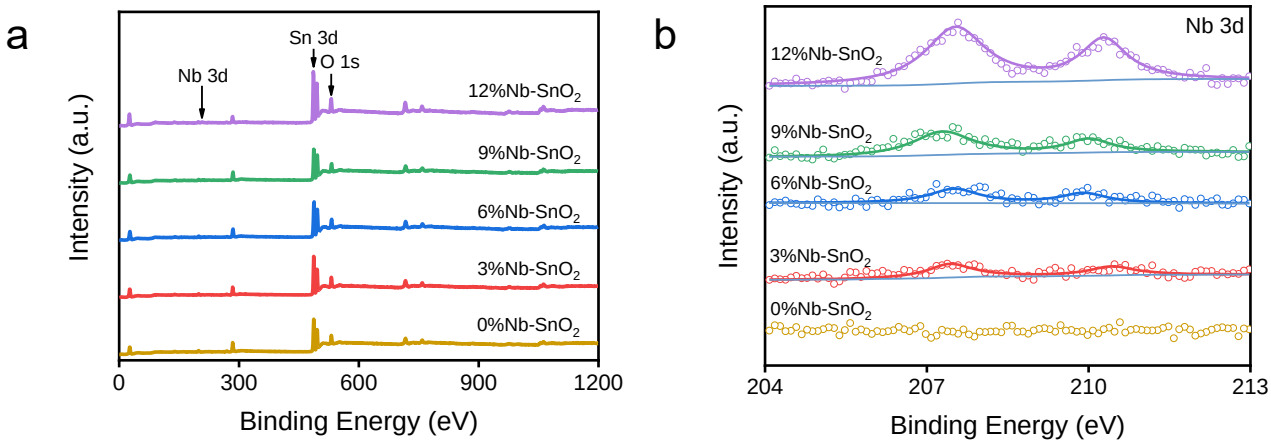

Fig. S3 XPS spectra of Nb-doped oxygen-deficient SnO_2 QDs: (a) survey and (b) Nb 3d.

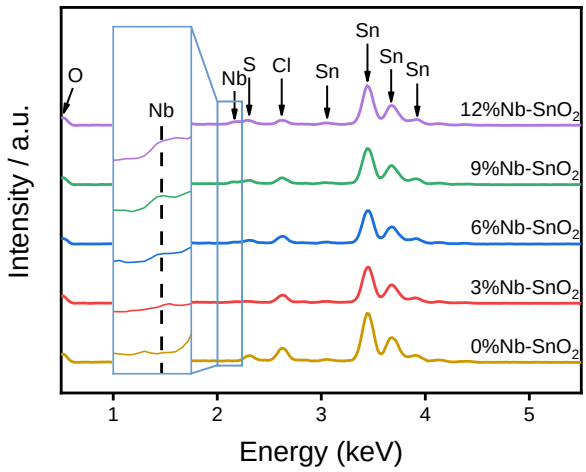

Fig. S4 EDS spectra of Nb-doped SnO_2 QDs when the Nb contents are 0%, 3%, 6%, 9% and 12% used in the experimental design.

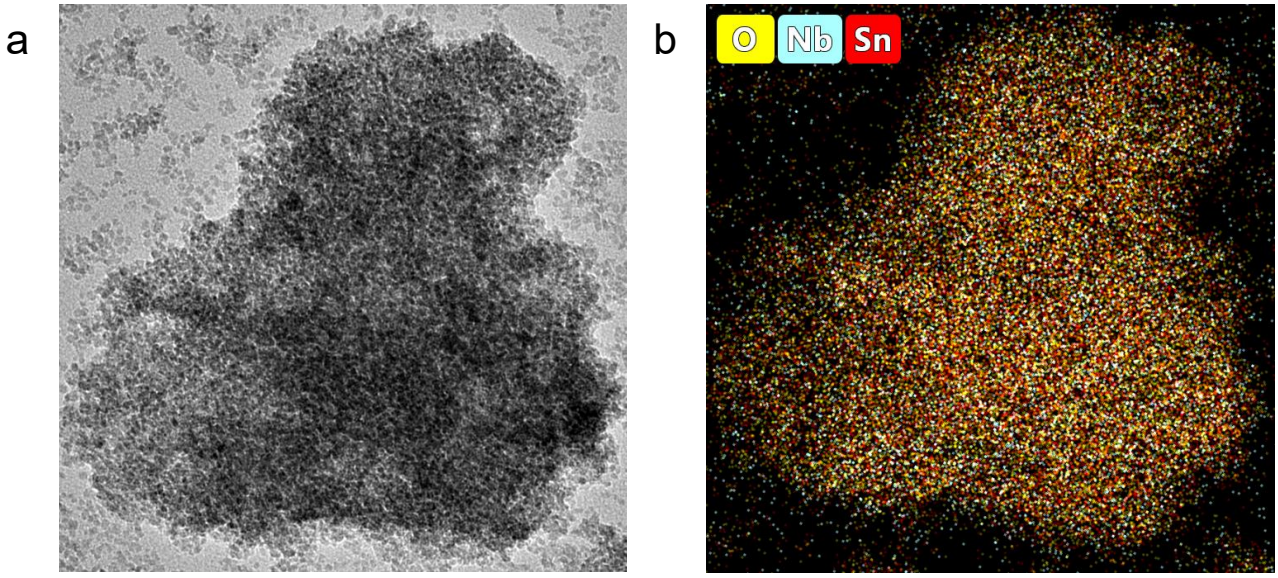

Fig. S5 HAADF-STEM elemental mapping of Nb-SnO_2 QDs.

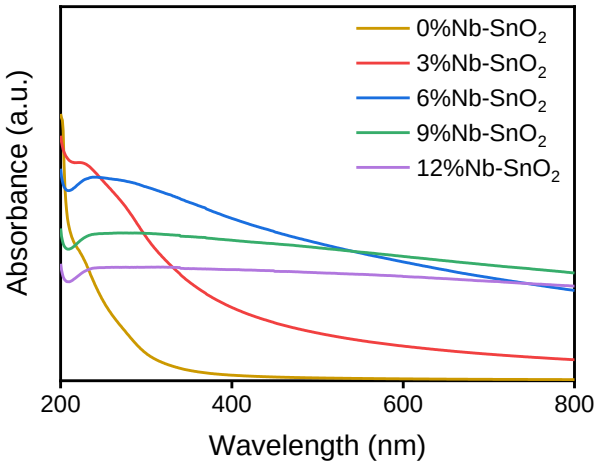

Fig. S6 UV-Vis absorbance of Nb-doped oxygen-deficient SnO_2 QDs.

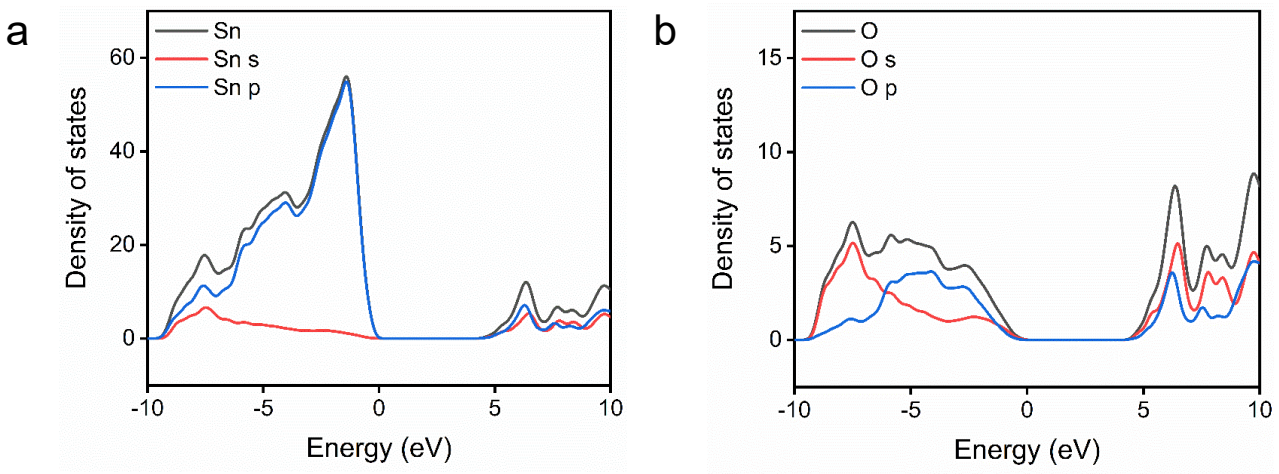

Fig. S7 Partial density of states in the undoped SnO_2 super cell with oxygen vacancies: (a) Sn and (b) O.

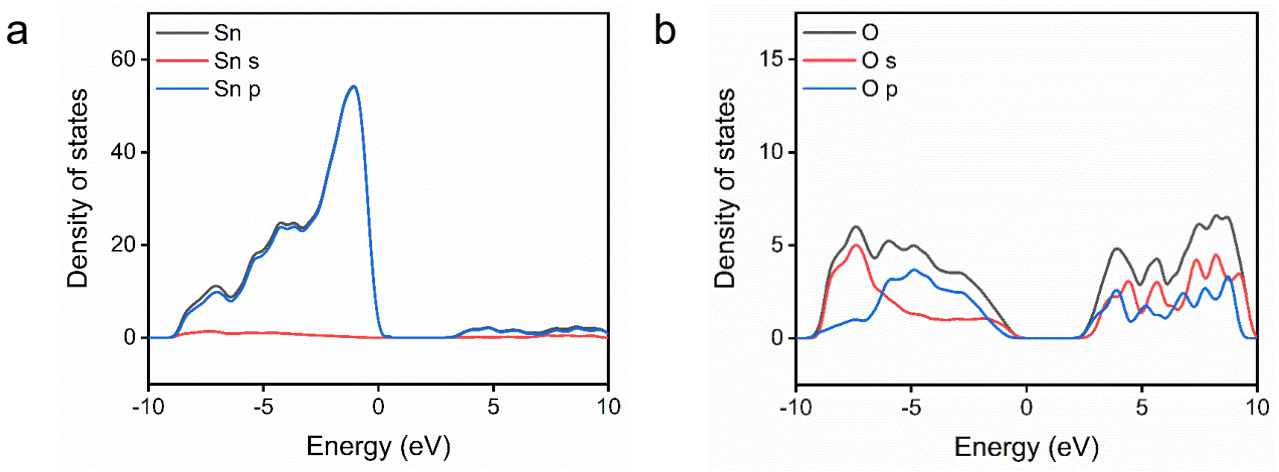

Fig. S8 Partial density of states in the Nb-doped SnO_2 super cell with oxygen vacancies: (a) Sn and (b) O.

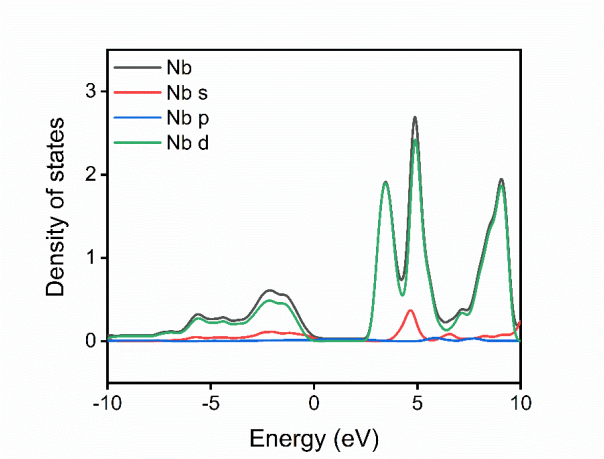

Fig. S9 Partial density of states of Nb in the Nb-doped SnO_2 super cell with oxygen vacancies.

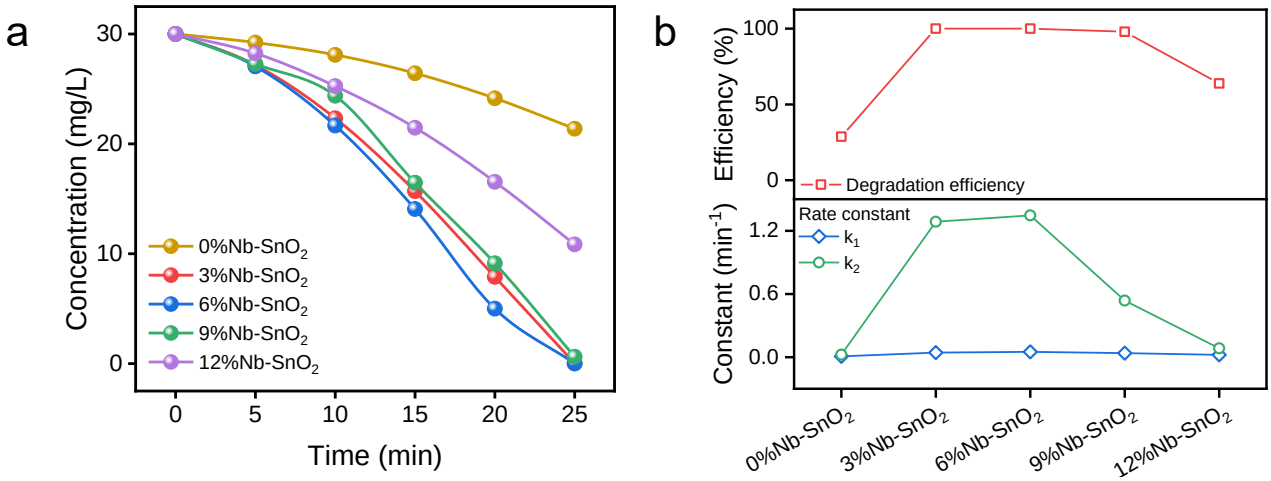

Fig. S10 Photocatalytic properties of Nb-doped SnO_2 QDs: (a) MO degradation in concentration; (b) influence of Nb addition amount on degradation efficiency and rate constants.

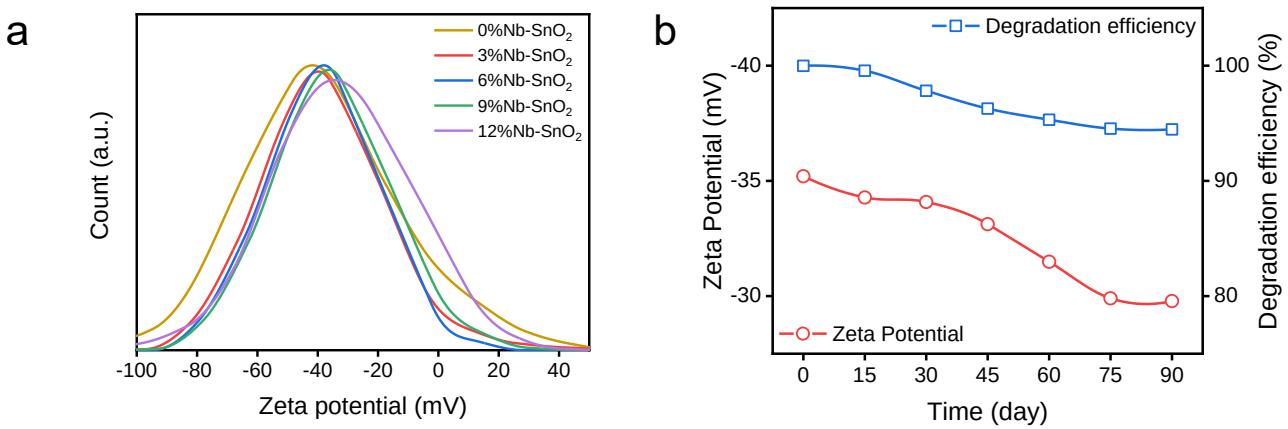

Fig. S11 (a) Zeta potentials of n%Nb-SnO_2 QDs in aqueous solution and (b) Long-term performances of 6%Nb-SnO_2 QDs in the aspects of Zeta potentials and efficiency of MO degradation.

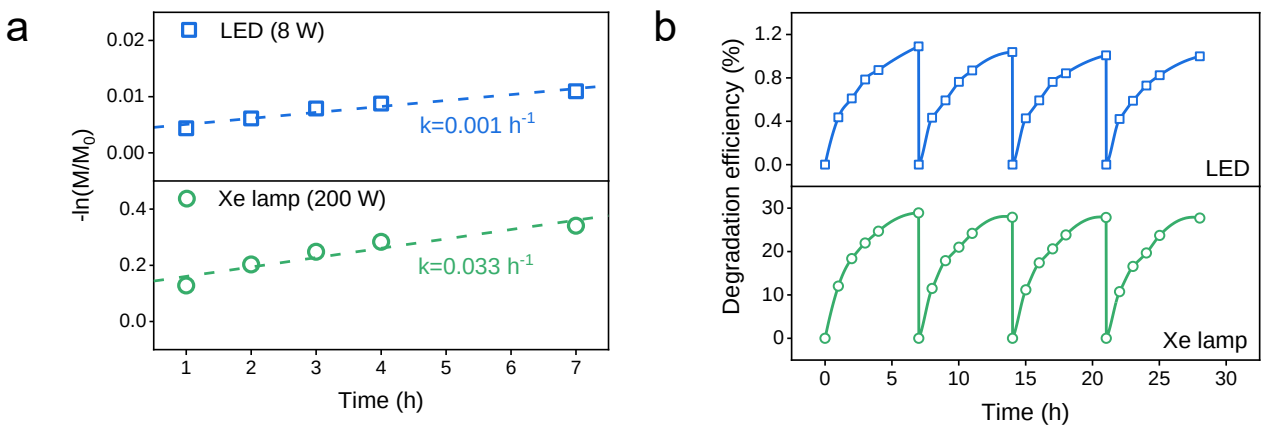

Fig. S12 Visible-light driven photocatalytic degradation of MPs by 6%Nb-doped SnO_2 QDs under the irradiation sources of LED and Xe lamp: (a) kinetics and rate constants; (b) Repeatability in 4 cycles.

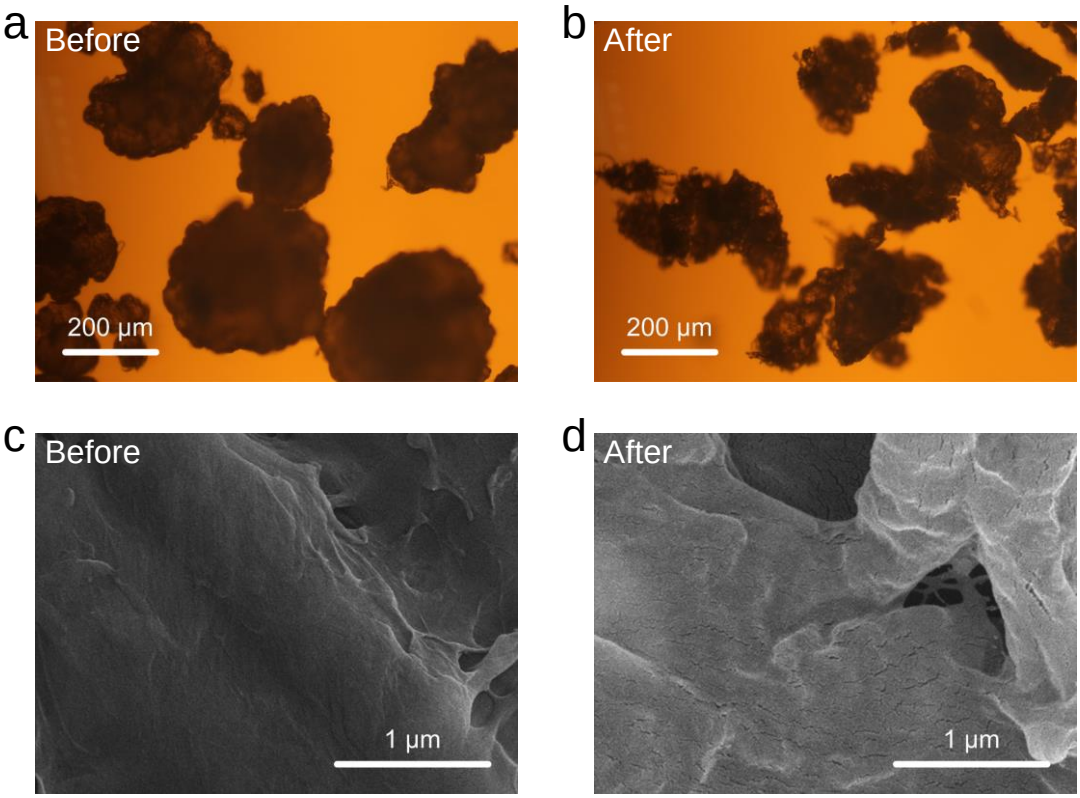

Fig. S13 PE morphology from (a-b) optical microscope and (c-d) SEM before and after photocatalytic activities.

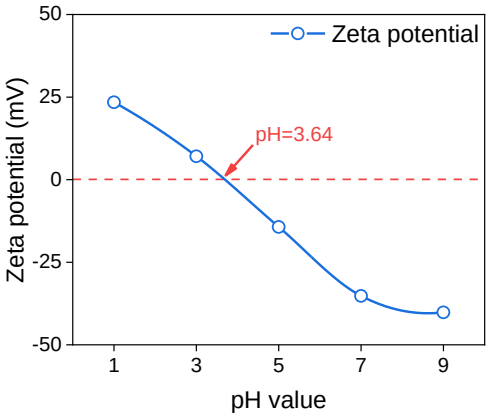

Fig. S14 The point of zero charge of the 6%Nb-doped SnO_2 QDs in aqueous solution.

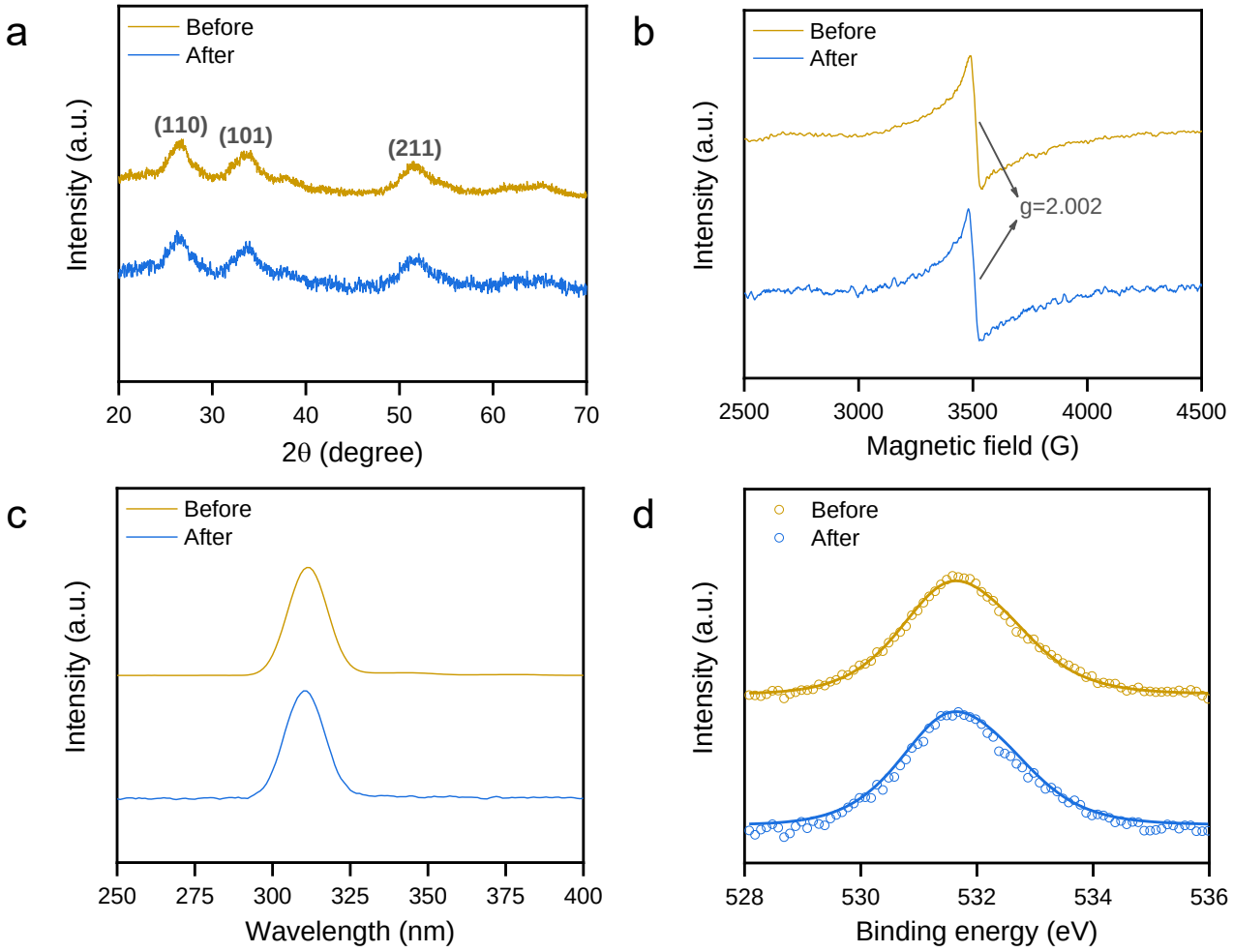

Fig. S15 Microstructural, compositional and optical characterizations of 6%Nb-SnO_2 QDs before and after photocatalytic degradation of MPs for 4 hours: (a) XRD patterns; (b) ESR spectra; (c) PL spectra and (d) XPS O 1s spectra.

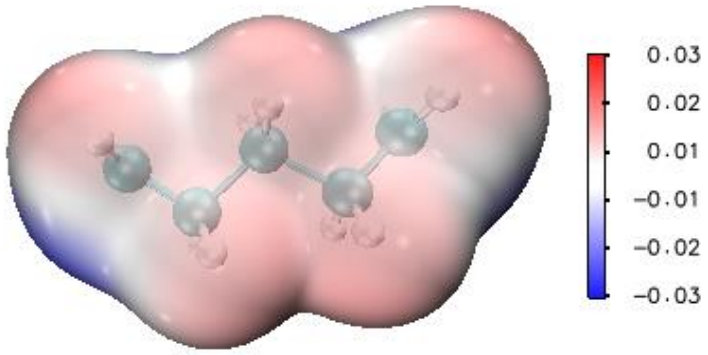

Fig. S16 The electrostatic potential distribution of PE microplastics.

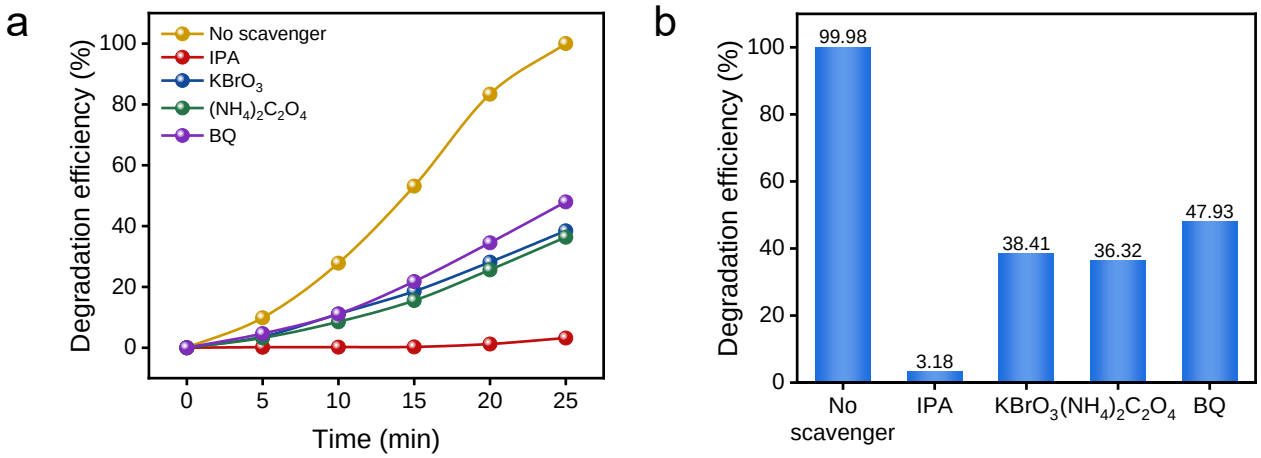

Fig. S17 Degradation efficiency in the trapping experiments for determination of primary active radicals in photocatalytic activities: (a) degradation efficiency over time; (b) degradation efficiency under various radical scavengers of IPA, $KBrO_3$, $(NH_4)_2C_2O_4$ and BQ.

Supplementary Tables

Table S1. Stoichiometry of Nb-doped oxygen-deficient SnO_2 QDs.

Sample	Nb/Sn	Sn/O	V_O percentage
0%Nb-SnO_2	0	0.565	11.4%
3%Nb-SnO_2	1.6	0.580	13.9%
6%Nb-SnO_2	3.05	0.598	16.4%
9%Nb-SnO_2	4.35	0.596	16.1%
12%Nb-SnO_2	5.7	0.595	16.0%

Table S2. Adsorption energies of various possible metal cations on the 6%Nb-SnO_2 supercell calculated by DFT computations.

Metal cation	Adsorption energy (eV)
Na^+	+0.057
K^+	+0.112
Ca^{2+}	+0.089
Mg^{2+}	+0.187
Zn^{2+}	+0.429
Cu^{2+}	+0.349
Fe^{3+}	+0.149
Al^{3+}	+0.184

Table S3. Comparison of visible-light driven photocatalytic degradation performances of MPs by semiconductors.

Photocatalyst	MPs	Radiation source wavelength	Radiation source power (W)	Degradation time (hour)	Degradation efficiency (%)	Performance (%/h/W)	Reference
N-doped TiO_2	PE	400-800 nm	27	20	6.64	0.0123	[74]
Fe-ZnO	LDPE	Visible light	105	120	25	0.0020	[75]
C,N-TiO_2	HDPE	Visible light	50	50	38	0.0152	[76]
TNT	LDPE	400-700 nm	85	1080	41	0.0004	[70]
BiOCl	HDPE	>420 nm	250	5	5.38	0.0043	[77]
N-TiO_2	LDPE	400-800 nm	50	50	4.65	0.0019	[78]
N-TiO_2	HDPE	400-800 nm	50	50	1.38	0.0006	[78]
C,N-TiO_2/SiO_2	PET	Visible light	50	120	16.22	0.0027	[79]
Cu_XO	PS	400-800 nm	50	50	23	0.0092	[80]
Nb-SnO_2	PE	400-800 nm	8	70	1.1	0.0195	This work
Nb-SnO_2	PE	380-1100 nm	200	70	28.9	0.0206	This work

Table S4. Intermediates of PE polyethylene degradation after 4-hour photocatalytic activity.

m/z	Product	Formula	Structure
422	Triacontane	$C_{30}H_{62}$	
312	Octadecanoic acid, ethyl ester	$C_{20}H_{40}O_2$	
284	Octadecanoic acid	$C_{18}H_{32}O_2$	
284	Hexadecanoic acid ethyl ester	$C_{18}H_{36}O_2$	
256	n-Hexadecanoic acid	$C_{16}H_{32}O_2$	
228	Tetradecanoic acid	$C_{14}H_{28}O_2$	
214	Tridecanoic acid	$C_{13}H_{26}O_2$	
128	Octanal	$C_8H_{16}O$	

Table S5. The photocatalytic properties of nNb-SnO_2 QDs in MO degradation.

Sample	Degradation efficiency (%)	Rate constant k_1 (min^{-1})	Rate constant k_2 (min^{-1})
0%Nb-SnO_2	28.73	0.008	0.024
3%Nb-SnO_2	99.96	0.043	1.286
6%Nb-SnO_2	99.98	0.050	1.346
9%Nb-SnO_2	97.93	0.038	0.537
12%Nb-SnO_2	63.84	0.022	0.084